JBC RESEARCH ARTICLE

Vascular endothelial profilin-1 drives a protumorigenic tumor microenvironment and tumor progression in renal cancer

Received for publication, April 18, 2023, and in revised form, July 6, 2023 Published, Papers in Press, July 13, 2023,
https://doi.org/10.1016/j.jbc.2023.105044

David Gau[1,*], Andrew Daoud[1], Abigail Allen[1], Marion Joy[2], April Sagan[2,3], Sanghoon Lee[2,3], Peter C. Lucas[2,4], Stefan Duensing[5], David Boone[3], Hatice U. Osmanbeyoglu[1,2,3,6], and Partha Roy[1,4,*]

From the [1]Department of Bioengineering, [2]UPMC Hillman Cancer Center, [3]Department of Biomedical Informatics, and [4]Department of Pathology, University of Pittsburgh, Pittsburgh, Pennsylvania, USA; [5]Department of Urology, University of Heidelberg School of Medicine, Heidelberg, Germany; [6]Department of Biostatistics, University of Pittsburgh, Pittsburgh, Pennsylvania, USA

Reviewed by members of the JBC Editorial Board. Edited by Enrique De La Cruz

Overexpression of actin-binding protein profilin-1 (Pfn1) correlates with advanced disease features and adverse clinical outcome of patients with clear cell renal carcinoma, the most prevalent form of renal cancer. We previously reported that Pfn1 is predominantly overexpressed in tumor-associated vascular endothelial cells in human clear cell renal carcinoma. In this study, we combined *in vivo* strategies involving endothelial cell–specific depletion and overexpression of Pfn1 to demonstrate a role of vascular endothelial Pfn1 in promoting tumorigenicity and enabling progressive growth and metastasis of renal carcinoma cells in a syngeneic orthotopic mouse model of kidney cancer. We established an important role of endothelial Pfn1 in tumor angiogenesis and further identified endothelial Pfn1-dependent regulation of several pro- (VEGF, SERPINE1, CCL2) and anti-angiogenic factors (platelet factor 4) *in vivo*. Endothelial Pfn1 overexpression increases tumor infiltration by macrophages and concomitantly diminishes tumor infiltration by T cells including CD8+ T cells *in vivo*, correlating with the pattern of endothelial Pfn1-dependent changes in tumor abundance of several prominent immunomodulatory cytokines. These data were also corroborated by multiplexed quantitative immunohistochemistry and immune deconvolution analyses of RNA-seq data of clinical samples. Guided by Upstream Regulator Analysis of tumor transcriptome data, we further established endothelial Pfn1-induced Hif1α elevation and suppression of STAT1 activation. In conclusion, this study demonstrates for the first time a direct causal relationship between vascular endothelial Pfn1 dysregulation, immunosuppressive tumor microenvironment, and disease progression with mechanistic insights in kidney cancer. Our study also provides a conceptual basis for targeting Pfn1 for therapeutic benefit in kidney cancer.

Renal cell carcinoma (RCC) accounts for ∼85% of all primary renal neoplasms. In 2023, the estimated new cases of RCC are 81,800 with 14,890 estimated deaths (1). RCC arises from the renal tubular epithelial cells, is heterogeneous in nature, and has several histologically and culary distinct subtypes. Clear cell RCC (ccRCC) is the most common subtype of RCC accounting for >75% of RCC cases. The other two major subtypes are papillary and chromophobe RCC that represent about 15 to 20% and 5% of RCC cases, respectively. Among the various subtypes of RCC, ccRCC has the worst clinical outcome with 20 to 30% of patients presenting metastasis at the time of diagnosis, development of local recurrence, or distant metastasis after initial surgery in one-third of patients. The median survival for patients with metastatic RCC patients is about 13 months with 5-years survival less than 10% (2, 3). The most common genetic alteration of ccRCC is the deletion of the short arm of chromosome 3 (3p) resulting in bi-allelic loss of a number of genes (Von-Hippel Lindau (VHL), PBRM1, BAP1, SETD2, KDM5C) at different frequencies. Loss of VHL is the most frequently (∼90%) encountered genetic aberration in ccRCC and plays a key role in initiation as well as progression of the disease. A major biological consequence of loss of VHL (encodes a ubiquitin ligase) is stabilization of isoforms of hypoxia-inducible factor (HIF1α and HIF2α) leading to overexpression of pro-angiogenic factors, such as vascular endothelial growth factor (VEGF) and creation of a highly vascularized tumor microenvironment (TME). These blood vessels are structurally abnormal marked by high tortuosity and hyperpermeability that promote hypoxia and immuno-suppressive TME, accelerating tumor progression. Apart from the surgical resection of the primary tumor, anti-angiogenic therapies primarily targeting VEGF signaling to promote vascular normalization are the first line therapy for ccRCC patients. However, almost all patients develop resistance and progression of drug-resistant disease (4–7).

We and others previously showed that overexpression of actin-monomer–binding protein profilin-1 (Pfn1) is a characteristic of advanced stage disease and lower overall survival and progression-free survival of ccRCC patients (8–12). Differential proteomic analyses identified Pfn1 to be within top 12 overexpressed proteins in metastatic *versus* primary RCC (10).

* For correspondence: Partha Roy, par19@pitt.edu; David Gau, dmg40@pitt.edu.

Although Pfn1 is ubiquitously expressed in almost all cell types, the Pfn1 protein is also processed/presented in major histocompatibility complex class I/II peptide complexes by cells in the RCC TME, but surprisingly not in normal adjacent kidney tissue, suggesting that Pfn1 may represent an RCC-associated antigen (13, 14). However, unlike many other types of cancers where Pfn1 expression is dysregulated in tumor cells, we demonstrated that Pfn1 expression is robustly upregulated at the transcriptional level in tumor-associated vascular endothelial cells (ECs) in human ccRCC (8). Pfn1's function is important for many actin-driven biological processes including vascular EC migration, proliferation, and angiogenesis (15–22). Although Pfn1 is primarily an intracellular protein, interestingly, various cells including EC cancer cells also secrete Pfn1 in the extracellular environment (8). Our previous *in vitro* studies suggested that vascular EC increases RCC cell migration through a paracrine mechanism of action and Pfn1 itself can be a potential extracellular mediator for EC-directed modulation of tumor cell behavior (8). The present study combines mouse model studies with clinical correlation findings to demonstrate for the first time an *in vivo* proof of a direct causal relationship between vascular endothelial Pfn1 dysregulation, alterations in TME, and disease progression in kidney cancer with mechanistic insights. Findings from our studies also provide a conceptual basis for justifying targeting Pfn1 for therapeutic benefit in kidney cancer.

Results

Vascular endothelial Pfn1 is an important driver of development and progression of kidney cancer

Among the three key histological subtypes of human RCC, Pfn1 expression is transcriptionally elevated in both ccRCC and papillary RCC (accounts for >90% of all RCC cases) with opposite trend observed in chromophobe, the least aggressive form of RCC (Fig. S1). Given prevalence of Pfn1 elevation in tumor-associated EC in ccRCC (the predominant form of RCC), we conducted syngeneic mouse model studies to assess the impact of selectively perturbing Pfn1 expression in EC on tumor development and progression in an orthotopic setting using RENCA, one of the most widely used Balb/c mouse-derived VHL+ RCC cell lines. CDH5-Cre$^{+/-}$ERT2 mouse is a well-established *in vivo* model to achieve knockout of a gene of interest selectively in EC cells in response to tamoxifen (23, 24).Therefore, for loss-of-function studies, we used our previously engineered Pfn1$^{flox/flox}$:CDH5-Cre$^{+/-}$ERT2 mice suitable for tamoxifen-induced excision of the *Pfn1* gene *via* the action of EC-restricted expression of Cre recombinase under a CDH5 (VE-cadherin) promoter (17). Since these mice were initially generated in a mixed genetic background, we backcrossed them for seven generations into a Balb/c background to create syngeneic compatible host for successful grafting of RENCA cells in our experiments. To assess the impact of loss of endothelial Pfn1 on tumorigenicity of RCC cells, we adopted a kidney-localized strategy for endothelial Pfn1 deletion (schematized in Fig. 1*A*). Specifically, we co-injected RENCA cells (pre-engineered to express luciferase [luc]) and adenovirus encoding either Cre (Ad-Cre: expresses Cre under an EC-selective CDH5 promoter) or GFP (Ad-GFP) as control in the kidney of Pfn1$^{flox/flox}$:CDH5-Cre-ERT2 mice and tracked tumor progression longitudinally by bioluminescence imaging (BLI) until their sacrifice on day 14. We prevalidated the efficiency of Ad-(CDH5)-Cre–mediated knockout of the Pfn1 gene in cultured MEC$^{Pfn1\text{-}fl}$ (an immortalized mouse kidney EC cell line that we generated from Pfn1$^{flox/flox}$ mice) with cells by 90% downregulation of Pfn1 expression relative to control Ad-GFP–transduced cells (Fig. S2*A*). The % reduction of Pfn1 at the protein level commensurates with the adenoviral infection efficiency as judged by % GFP positivity of cells. Since our *in vivo* experiments involved exogenous Ad-Cre–mediated deletion of the *Pfn1* gene, tamoxifen administration was not necessary, and the Cre genotype status was not a factor for selection of the recipient mice for these studies. A significant subset of Ad-Cre–administered mice (3 out of 7) failed to initiate macroscopic tumor and accordingly exhibited no detectable BLI signal even after 14 days (Fig. 1, *B* and *C*). The mean tumor burden (expressed as the weight of the tumor-bearing kidney normalized to that of uninvolved contralateral kidney) of Ad-Cre recipient mice was significant lower than that of Ad-GFP recipient mice (Fig. 1*D*). Reverse transcription-polymerase chain reaction (RT-PCR) analyses of tumor samples confirmed Cre expression *in vivo* (inset of Fig. 1*D*). Immunohistochemical costaining of tumor sections for CD31 (an EC marker) and Pfn1 further confirmed EC specificity for loss of Pfn1 expression in Ad-Cre–administered tumors (Fig. S2*B*). As expected, lung histology showed significantly more prominent metastases of RENCA cells in Ad-GFP relative to Ad-Cre recipient mice (Fig. 1, *E* and *F*). As a complementary gain-of-function experiment, we next investigated the effect of EC-specific Pfn1 overexpression on tumorigenic ability of RCC cells. For these studies, we co-injected RENCA cells with adeno-associated virus (AAV) to express either Pfn1 (AAV-Pfn1, also co-expresses mCherry as a reporter) or RFP (AAV-RFP; control) under a CDH5 promoter, into the kidney of Balb/c mice, and tracked tumor progression longitudinally by BLI (schematized in Fig. 2*A*). We selected AAV1 serotype for efficient transduction of vascular EC (25) and prevalidated the ability of AAV-CDH5-Pfn1 to upregulate Pfn1 expression when transduced in cultured MEC$^{Pfn1\text{-}fl}$ cells (Fig. S3). Consistent with our loss-of-function mouse model data and Pfn1 overexpression in human RCC, AAV-Pfn1 administration significantly accelerated the primary tumor growth and lung metastasis of RENCA cells (Fig. 2, *B*–*F*). RT-PCR analyses of tumor samples confirmed AAV-mediated expression of mCherry/RFP *in vivo* (inset of Fig. 2*D*). Together, these loss- and gain-of-function studies demonstrate that endothelial Pfn1 promotes tumorigenic ability of RCC cells.

Next, to determine whether progressive growth in RCC is dependent on endothelial Pfn1, we pre-established kidney tumors by injecting RENCA cells in Pfn1$^{flox/flox}$:CDH5-

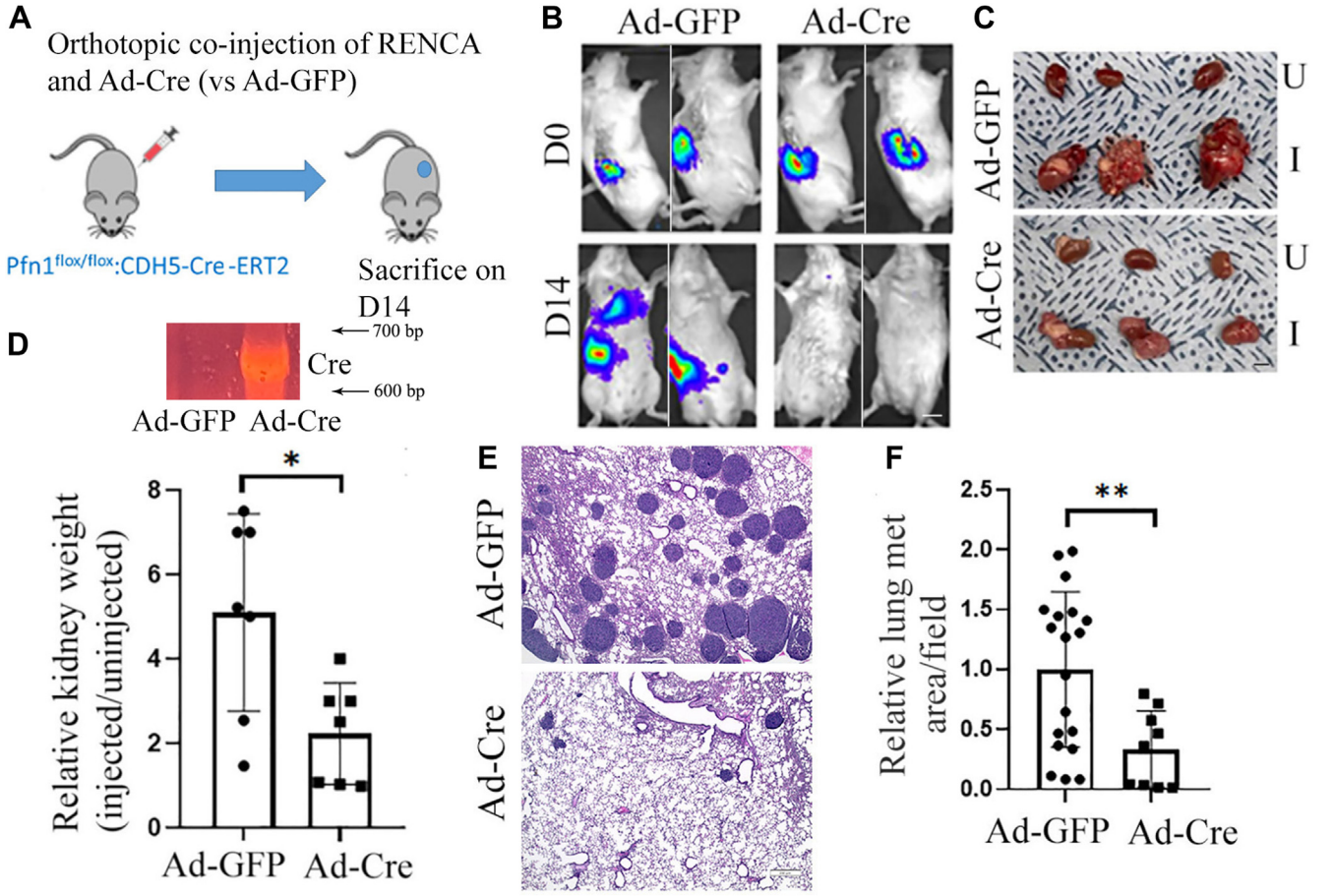

Figure 1. Effect of kidney-localized deletion of endothelial Pfn1 on tumorigenicity and lung metastasis of RCC cells. *A*, schematic representation of the experimental protocol. *B–F*, representative bioluminescence images of injected mice belonging to the indicated group on day 0 and day 14, and images of kidneys [tumor cell injected (I) *versus* contralateral uninvolved (U)] harvested on day 14 are shown in (*B* and *C*), respectively [scale bar represents 1 cm (*B*), scale bar represents 500 μm (*C*)]. *D*, shows the relative tumor burden data between the two groups summarized from seven mice/group pooled from two independent experiments. The DNA gel in the inset of (*D*) shows Cre amplicon in tumor RT-PCR product only in Ad-Cre–inoculated tumor confirming adenovirus-mediated Cre expression *in vivo*. Representative H&E staining of lungs harvested on day 14 to demonstrate prominent difference in metastases between the two groups (*E*); quantification of metastases (based on 2–3 lung sections/animal) affected area are shown alongside in (*F*) (data normalized to the mean value of Ad-GFP treatment group) (*$p < 0.05$; **$p < 0.01$; scale bar represents 200 μm). RCC, renal cell carcinoma.

$Cre^{+/-}$ERT2 mice as before. After 7 days, we initiated a five consecutive day course of tamoxifen administration to induce widespread endothelial Pfn1 gene excision (these mice are referred to as $Pfn1^{EC(-/-)}$ hereon) as schematized in Figure 3*A*. Littermate control $Pfn1^{+/+}$ mice (either Cre-negative with any Pfn1 genotype or harbored WT Pfn1 alleles) were also injected with RENCA cells and subjected to tamoxifen administration in an identical manner. We preferred this widespread deletion strategy over Ad-Cre–mediated kidney-restricted deletion for these proof-of-concept studies mainly due to the practical inconvenience of two successive invasive kidney injection within a span of 7 days associated with the local deletion approach. However, we have also found that widespread endothelial loss of Pfn1 even in nontumor-bearing mice causes multi-organ pathology and inflammation requiring compassionate euthanasia of the animals about 18 to 21 days from the last day of tamoxifen administration (manuscript under consideration). Being cognizant of this biological limitation, we terminated our tumor progression experiments on day 24 (counted from the day of tumor cell inoculation) when no obvious sign of distress was evident in $Pfn1^{EC(-/-)}$ mice (this is at least a week prior to the anticipated timeline of death of these animals). We found that triggering endothelial Pfn1 deletion results in significant decrease in end point primary tumor burden with macroscopic tumors not even detected in two out of seven mice at the necropsy (Fig. 3, *B* and *C*), suggesting that endothelial Pfn1 is also critical for progressive growth of RCC cells *in vivo*. H&E staining revealed presence of extensive necrosis in both primary tumor and lung metastases in $Pfn1^{EC(-/-)}$ mice suggesting cell death likely ensuing this phenotype (Fig. 3*D*). Collectively, these mouse model data underscore an important role of vascular endothelial Pfn1 in driving tumor development and progression in RCC.

Endothelial Pfn1 loss causes impairment in tumor angiogenesis in mouse model of RCC

Previous studies found that VEGF stimulates Src-dependent phosphorylation of Pfn1 on its tyrosine 129 (Y129) residue,

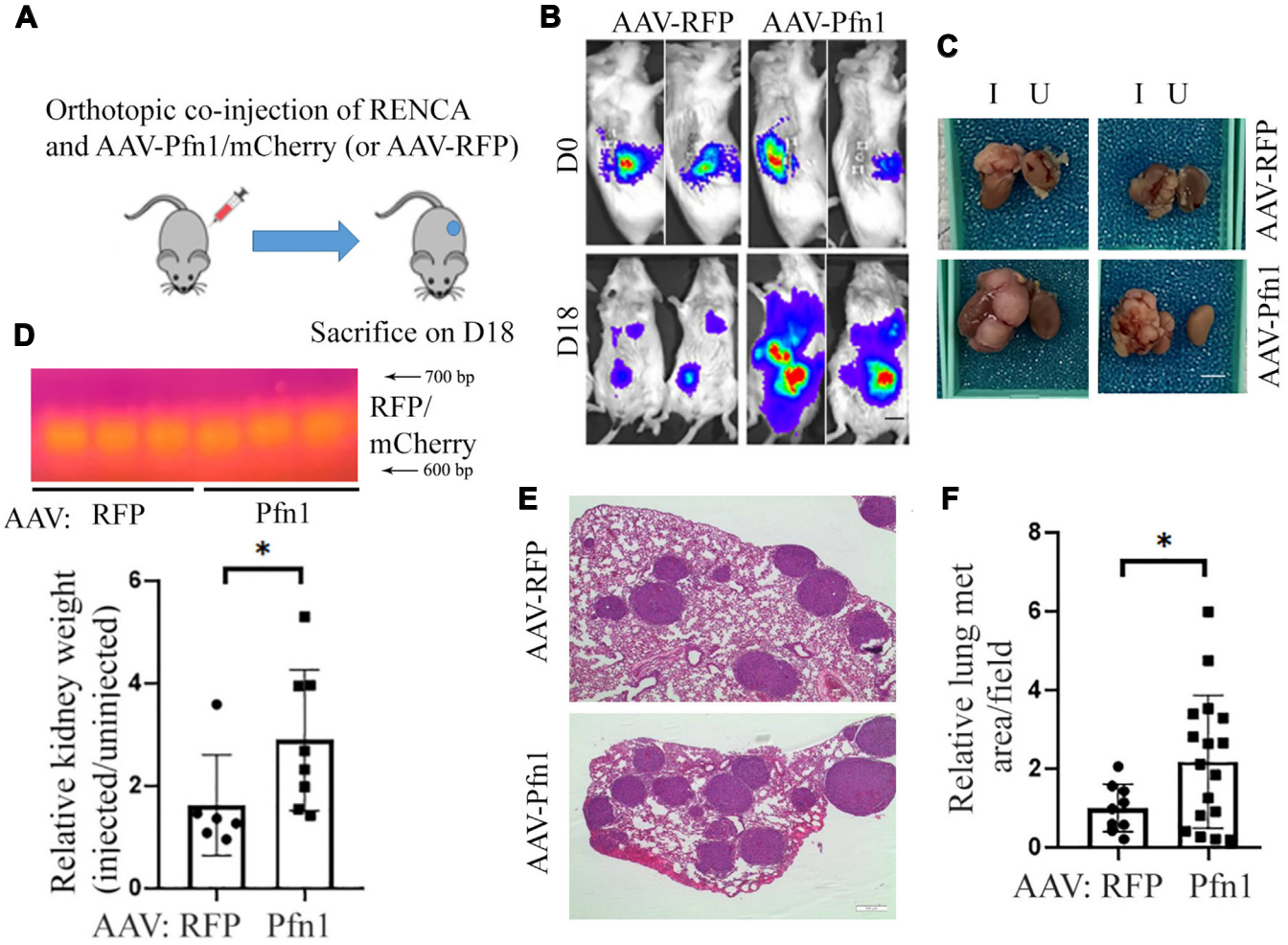

Figure 2. Effect of kidney-localized overexpression of endothelial Pfn1 on tumorigenicity and lung metastasis of RCC cells. *A*, schematic representation of the experimental protocol. *B–F*, representative bioluminescence images of injected mice belonging to the indicated group on day 0 and day 18, and images of kidneys [injected (I) *versus* contralateral uninvolved (U)] harvested on day 18 are shown in (*B* and *C*), respectively [scale bar represents 1 cm (*B*), scale bar represents 500 μm (*C*)]. *D*, shows the relative tumor burden data between the two groups summarized from 6 to 8 mice/group pooled from two independent experiments. The DNA gel in the inset of (*D*) shows RFP/mCherry amplicons in tumor RT-PCR product confirming AAV-mediated transgene expression *in vivo*. Representative H&E staining of lungs harvested on day 18 to demonstrate difference in metastases between the two groups (*E*); quantification of metastases (based on evaluation of 2–3 lung sections/animal) affected area are shown alongside in (*F*) (data normalized to the mean value of AAV-RFP treatment group) (*$p < 0.05$; scale bar represents 200 μm). AAV, adeno-associated virus; RCC, renal cell carcinoma.

and this phosphorylation increases Pfn1's affinity for actin. Although blocking this phosphorylation (through substitution of Y for F) does not diminish the basal Pfn1–actin interaction, it reduces tumor angiogenesis in glioblastoma setting (21, 22). More recently, we showed that tamoxifen-induced triggering of deletion of endothelial Pfn1 during early postnatal phase in $Pfn1^{flox/flox}$:CDH5-Cre-ERT2 mice leads to an impairment in retinal vascular development, establishing Pfn1's requirement for developmental angiogenesis (17). Whether tumor angiogenesis is also susceptible to loss of endothelial Pfn1 expression is not known. Therefore, we performed CD31 immunohistochemistry (IHC) of RENCA tumors harvested from Pfn1 deletion and overexpression studies. We found a significant ∼50% reduction in CD31+ areas in Ad-Cre– relative to Ad-GFP–administered tumors ($p < 0.01$) (Fig. 4, *A* and *B*). These data are also consistent with diminished RENCA-induced angiogenesis in subcutaneously implanted matrigel plugs when endothelial Pfn1 gene is globally disrupted (Fig. S4). Surprisingly, however, there was no significant difference in CD31+ area between AAV-RFP– and AAV-Pfn1–administered tumors (Fig. 4, *C* and *D*). These results suggest that while endothelial Pfn1 is required for tumor angiogenesis in RCC, increasing Pfn1 beyond a certain level does not further augment the angiogenic capability of EC.

Endothelial Pfn1 promotes increased infiltration of macrophages into the RCC TME while reducing infiltration of CD8 T cells in mouse model of RCC

Since our mouse model studies showed that endothelial Pfn1 overexpression accelerates RCC progression without stimulating tumor angiogenesis, we postulated that endothelial Pfn1 may promote tumor progression by altering some other aspects of TME. Given that immune cells play a key role in defining protumorigenic *versus* antitumorigenic TME, we next analyzed macrophage and T cell infiltration in RENCA tumors harvested from Pfn1 overexpression and knockout studies by

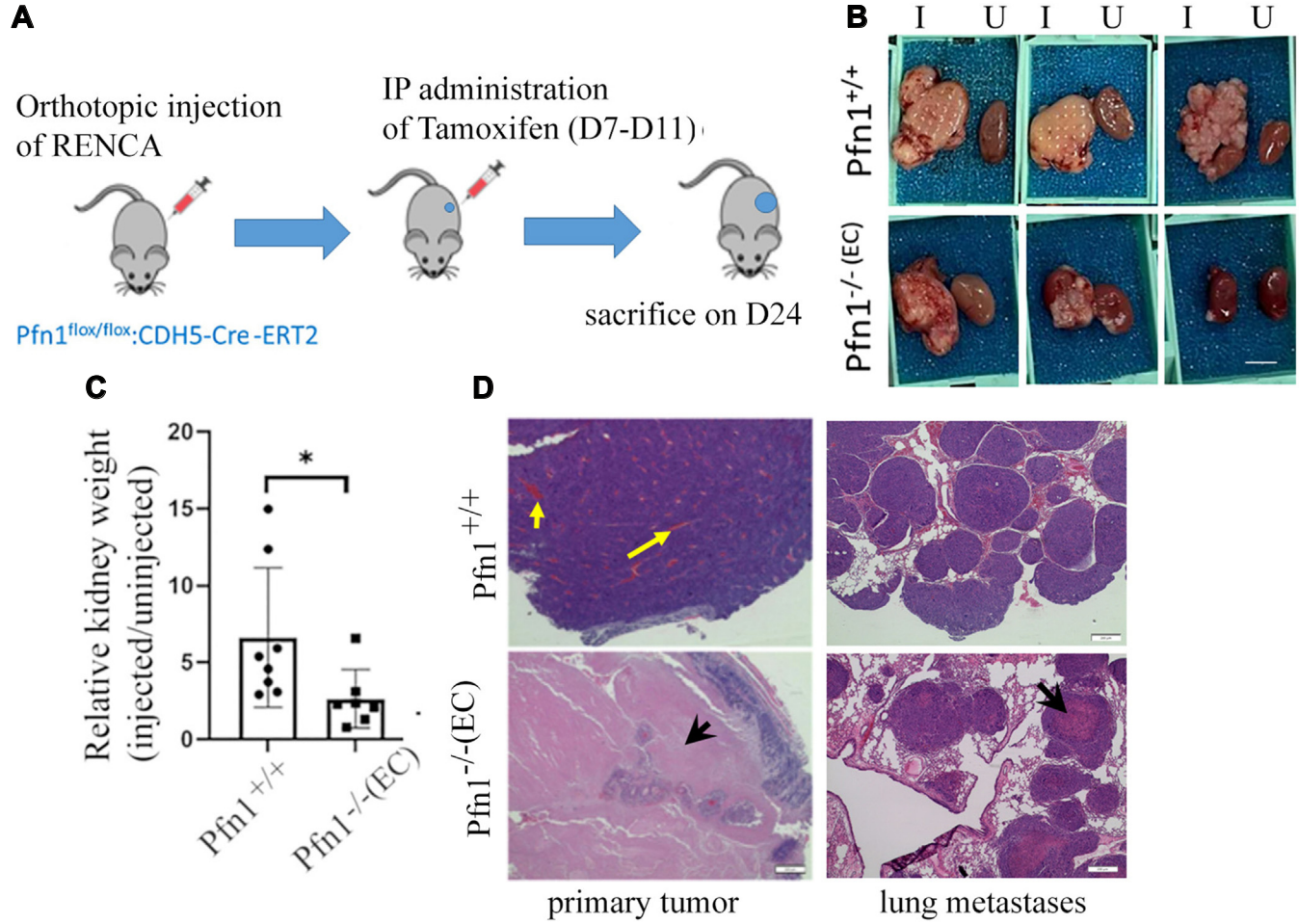

Figure 3. Effect of widespread deletion of endothelial Pfn1 on progressive growth of RCC cells *in vivo*. *A*, schematic representation of the experimental protocol. *B–D*, representative images of harvested kidneys [injected (I) *versus* contralateral uninvolved (U)] at the necropsy are shown in (*B*) (scale bar represents 500 μm). *C*, shows the relative tumor burden data between the two groups summarized from 7 to 8 mice/group pooled from two independent experiments. Representative H&E staining (*D*) of kidneys and lungs show extensive necrosis (*arrowheads*) in both primary tumor and lung metastases specifically in $Pfn1^{-/-(EC)}$ mice (*yellow arrows*: tumor-associated blood vessels). Note that the number of metastases were also fewer in $Pfn1^{-/-(EC)}$ relative to $Pfn1^{+/+}$ mice (*$p < 0.05$; scale bar represents 200 μm). EC, endothelial cell; RCC, renal cell carcinoma.

quantitative IHC using antibodies against F4/80 (a macrophage marker), CD3 (a general T cell marker), and CD8 (an effector T cell marker). We found that endothelial Pfn1 overexpression leads to increased tumor infiltration by macrophages with concomitant reduction of intratumoral abundance of CD3+ as well as CD8+ T cells (Fig. 4, *E–J*). Consistent with these data, Ad-Cre–administered tumors showed a significant 25% reduction in F4/80+ area relative to Ad-GFP–administered tumors, but CD3 staining did not detect any significant change in intratumoral T cell abundance between the two experimental conditions (Fig. S5).

Clinical corroboration of endothelial Pfn1's effect on immune microenvironment in RCC

To establish clinical relevance of our mouse model findings, we next queried endothelial Pfn1's relation to tumor infiltration by macrophages and T cells in the clinical samples of RCC by several approaches. First, we performed immune deconvolution of the TCGA (The Cancer Genome Atlas) bulk RNAseq data of 535 human ccRCC tumors using CIBERSORTx. These analyses revealed positive and negative correlations between bulk tumor Pfn1 mRNA expression and predicted tumor abundance of macrophages and B cells, respectively (Fig. 5*A*). In particular, Pfn1 expression was found to have strongest positive correlation with MKI67+ (a marker generally correlated with an immune-exhausted TME (26)) subpopulation of macrophages. Based on the Spearman's correlation values, the association of Pfn2 (an isoform that is closest relative to Pfn1) with tumor infiltration by various immune cells was negligible compared to that seen for Pfn1. However, a positive correlation between Pfn1 expression and predicted tumor abundance of CD8+ T cells in immune deconvolution analyses of the TCGA data (Fig. 5*A*) appeared contradictory to our mouse model findings.

A key caveat of immune deconvolution of bulk RNAseq data is that these findings are heavily skewed by gene expression in tumor cells. Furthermore, mRNA expression data do not always correlate with protein data. Therefore, to specifically probe for the effect of endothelial Pfn1 expression at the protein level on

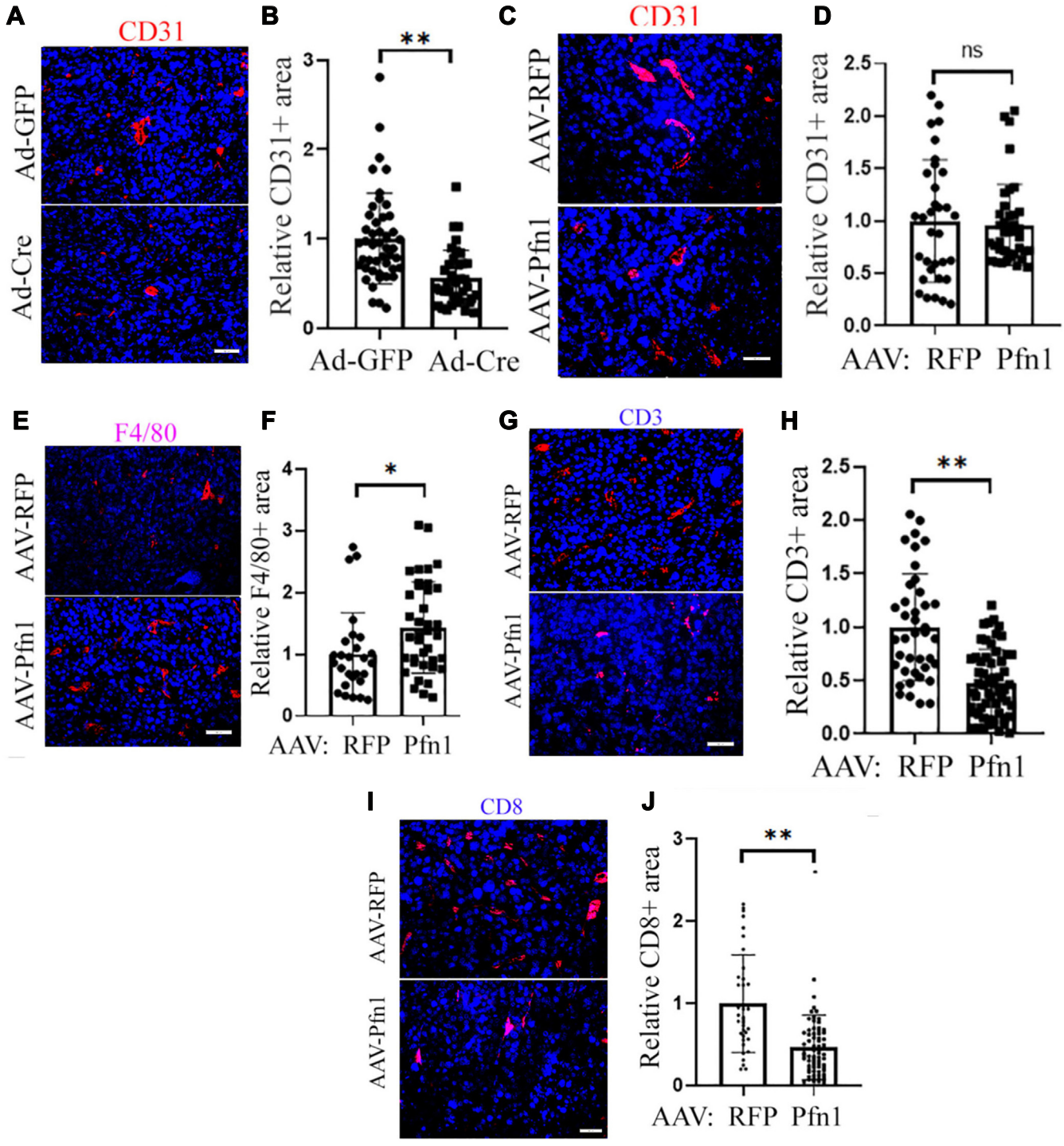

Figure 4. Effect of kidney-localized endothelial Pfn1 perturbation on tumor angiogenesis and tumor infiltration by immune cells in mouse model of RCC. *A–D*, representative CD31 and DAPI costaining images CD31+ area of histosections of Ad-Cre– (*A*) and AAV-Pfn1–administered (*C*) RENCA tumors and the associated quantifications relative to their respective control groups (*B* and *D*). *E–J*, representative images of F4/80, CD3, and CD8 staining (with DAPI counterstaining) of AAV-Pfn1 *versus* AAV-RFP (control) co-administered RENCA tumors and the associated quantifications (relative to AAV-RFP group). Data are summarized from analyses of at least 25 10×-field images acquired from multiple sections of four tumors from each group from gene deletion and overexpression experiments (*$p < 0.05$; **$p < 0.01$; scale bar represents 200 μm). AAV, adeno-associated virus; RCC, renal cell carcinoma.

immune microenvironment in human RCC, we next performed multiplexed quantitative IHC of tissue microarrays (TMAs) containing a large cohort (n = 191 tumors) of RCC tumors (predominantly comprised of ccRCC histology). Specifically, we stained the TMAs with antibodies specific for Pfn1, pan-cytokeratin (CK—to distinguish tumor cells from stromal cells), CD31, CD68 (macrophage marker), CD8 (effector T-cell marker), and FOXP3 (Treg marker) along with nuclear marker

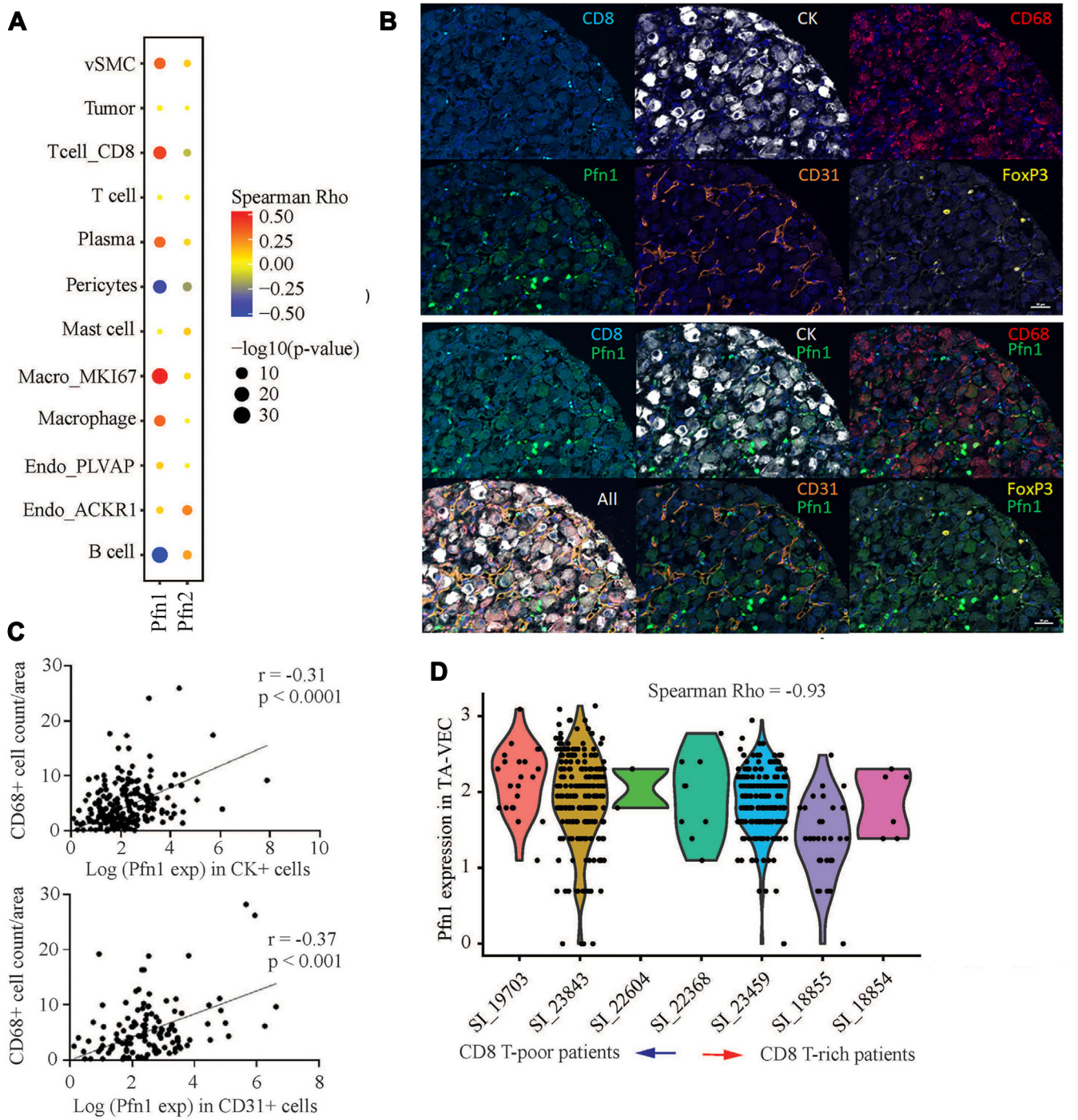

Figure 5. Association between Pfn1 expression and tumor infiltration by immune cells in clinical samples of RCC. *A*, a graphical summary depicting correlation between estimated cell type fractions with mRNA expression of Pfn1 and its closest isoform Pfn2 based on CIBERSORTx transcriptome deconvolution analyses of bulk RNAseq data of ccRCC tumors (source: TCGA, n = 535). *B*, representative images of multiplexed IHC of a randomly selected region of an RCC TMA spot showing TME stained for various markers including Pfn1, CD31, CD8, CD68, FoxP3, pan-cytokeratin (CK), and DAPI. The *upper* and *lower panels* show individual cell type images without or with superimposition of Pfn1 (scale bar represents 30 μm). *C*, positive correlation between tumor infiltration by CD68+ macrophages (defined by CD68 staining intensity) and the average TMA Pfn1 expression in either CK+ tumor cells or CD31+ tumor-associated EC cells (each dot represents an individual tumor sample; r = Pearson's coefficient). This is based on the analyses of a total of 191 spots pooled from multiple TMAs. *D*, a violin plot showing Pfn1 expression in ACKR1+ subset of tumor-associated vascular EC (VEC) in CD8 T cell-poor *versus* CD8-T cell-rich ccRCC tumors (based on the analyses of scRNAseq data of seven ccRCC patients; GSE159115). CD8 T cell fraction was calculated in each of these seven patients, and the patients are displayed from *left* to *right* in an ascending order of CD8 T cell fraction. Spearman's correlation coefficient rho was calculated between Pfn1 expression in ACKR1+ TA-VEC and CD8 T cell fraction. ACKR1, atypical chemokine receptor 1; ccRCC, clear cell renal carcinoma; EC, endothelial cell; IHC, immunohistochemistry; RCC, renal cell carcinoma; TCGA, The Cancer Genome Atlas; TMA, tissue microarray; TME, tumor microenvironment.

DAPI (Fig. 5*B*). Individual TMA spot analyses revealed significant positive correlation between tumor infiltration by macrophages and average Pfn1 expression in either CD31+ tumor-associated EC (Pearson's coefficient = 0.37; $p < 0.001$) or CK+ tumor cells (Pearson's coefficient = 0.31; $p < 0.0001$) (Fig. 5*C*). For spatial information of various cellular types in the RCC

TME, we additionally performed cellular neighborhood analyses on the entire set of multiplexed TMA images choosing 100 μm as the size of the region. These analyses identified five distinct classes of cellular neighborhoods: 0 (bulk tumor), 1 (high macrophage-infiltrated tumor), 2 (EC-enriched, moderate macrophage-infiltrated tumor), 3 (moderate macrophage infiltrated tumor), and 4 (T cell– and moderate macrophage-infiltrated tumor) (Fig. S6*A*). As per these analyses, endothelial Pfn1 expression in neighborhoods enriched in macrophage infiltration (neighborhoods 1 through 4) was found to be higher relative to one with negligible macrophage abundance (neighborhood 0) (Fig. S6*B*). The distinction became more evident when macrophage counts were binned where a clear positive trend was detected between endothelial Pfn1 expression and the number of macrophages detected within a 100 μm TME region (Fig. S6*C*). Overall, these immune deconvolution and TMA analyses data further consolidated our mouse model findings to support a role of endothelial Pfn1 in promoting tumor infiltration by macrophages.

We also analyzed TMA data to query Pfn1 expression in either endothelial or tumor cell compartment has any association with tumor infiltration by either effector or regulatory T cells. Since a significantly large fraction (∼75%) of TMA spots were found to be almost devoid of CD8+ and FOXP3+ cells over a broad range of Pfn1 expression, instead of performing correlation analyses, we compared CD8 T cell and Treg abundance between $Pfn1^{low}$ and $Pfn1^{high}$ tumors in a cell type–specific manner with Pfn1 expression dichotomized at the median value. As per these analyses, CD8 T cell abundance in the TME, if at all, was found to be modestly (but significantly) higher in tumors associated with higher endothelial Pfn1 expression relative to those with lower endothelial Pfn1 expression (Fig. S7*A*), contradicting our mouse model data. However, tumors with $Pfn1^{high}$ CK+ cancer cells exhibited modestly lower infiltration of CD8 T cells relative to those with $Pfn1^{low}$ CK+ cancer cells (Fig. S7*A*). We did not find any effect of Pfn1 expression in either cellular compartment on tumor infiltration by Tregs (Fig. S7*B*).

We considered several limitations of the TMA studies that could possibly account for discordant result between the TMA and the mouse model studies with regard to endothelial Pfn1's effect on tumor infiltration by CD8 T cells. First, single-core TMA image analysis does not capture the complexity of tumor heterogeneity and its impact on T-cell infiltration. Second, mixed tumor histology can be a confounding factor. Third, single-cell RNAseq data have revealed transcriptomic heterogeneity of tumor-associated EC in human ccRCC (27), which was not accounted for in TMA studies. Therefore, we next performed analyses of publicly available single-cell RNAseq transcriptome dataset (GSE159115) of ccRCC tumors (N = 7 patients reported in (27)). Interestingly, these analyses revealed a striking negative correlation (Spearman's coefficient: −0.93) between Pfn1 expression in a subset of tumor-associated EC that are positive for ACKR1 (atypical chemokine receptor 1) expression and tumor infiltration by CD8+ T cells (Fig. 5*D*), recapitulating our mouse model data from endothelial Pfn1 overexpression studies.

Endothelial Pfn1 perturbation impacts tumor abundance of angiogenic and immunomodulatory factors

To gain further mechanistic insight into the molecular basis for angiogenesis defect in an endothelial Pfn1-KO setting, we analyzed tumor lysates (three tumors per experimental group) prepared from both knockout and overexpression studies to probe for changes in pro- and anti-angiogenic factors using a 53-plex angiogenesis array. With a minimum of mean 1.5 fold change set as a cut-off, we found lower abundance of several pro-angiogenic factors (SerpinE1, VEGF, TIMP1, MIP1α/CCL3, matrix metalloproteinase (MMP)3, MCP-1/CCL2, KC/CXCL1) and one anti-angiogenic factor (platelet factor 4, PF4) in Ad-Cre tumors relative to Ad-GFP tumors (Fig. 6, *A* and *B*). SerpinE1, VEGF, and PF4 ranked the top three factors with SerpinE1 showing the most robust (3-fold) reduction in expression upon loss of endothelial Pfn1. Tumor abundance of all of these factors except MMP3 and CXCL1 showed opposite trends in their tumor abundance when endothelial Pfn1 is overexpressed (Fig. 6, *C* and *D*). However, we were also able to identify upregulation of many additional factors in the overexpression setting including highly prominent pro-angiogenic (*e.g.*, FGFs, SDF1, and endoglin) as well as anti-angiogenic (endostatin) factors. The factors which showed the most robust increase (>4-fold) were SerpinE1 (4.8-fold), PF4 (6.59-fold), endostatin (4.9-fold), CCL2 (4.98-fold), endoglin (6.46-fold), and VEGF (4.91-fold). In summary, based on the directional consistency and overlap of factors between the two experimental settings and the magnitude of the protein fold change, VEGF, SerpinE1, and CCL2 appear to be the most heavily impacted angiogenesis-stimulating factors in the RCC TME upon endothelial Pfn1 perturbation *in vivo*.

Given our multiple lines of evidence supporting the role of endothelial Pfn1 in stimulating tumor infiltration by macrophages, we next performed immunomodulatory cytokine/chemokine profiling (using a 31-plex Luminex-based array) of Ad-Cre *versus* Ad-GFP tumors (three tumors per group). In parallel, we performed transcriptional profiling of these tumors (three tumors/group) by bulk RNA-seq to orthogonally validate the luminex data and gain additional insights into endothelial Pfn1-dependent changes in gene expression and biological pathways *in vivo*. Differentially expressed genes (DEGs) were selected based on the absolute fold change in expression >1.5 from RNA-seq studies with the cut-off value for the false discovery rate set to 0.05. With these criteria, we found a total of 595 DEGs (340 upregulated and 255 downregulated) between Ad-GFP– *versus* Ad-Cre–treated tumors (Fig. 7*A*; top 50 upregulated and downregulated genes are listed in Table S1). Both RNA-seq and Luminex analyses of tumors revealed that loss of endothelial Pfn1 leads to reduction in tumor abundance of several major cytokines that are known to recruit and polarize macrophage into an anti-inflammatory M2-like phenotype (*e.g.*, CXCL1, CCL3, CCL4, CXCL2, and VEGF) and, concomitantly, increases abundance of potent T-cell recruiting cytokines (CXCL10, CXCL9, and CCL5) in the RCC TME (Fig. 7*B*). Luminex studies revealed reduction of few additional cytokines in Ad-Cre relative to Ad-GFP tumors including G-CSF, IL6, and LIF (a cytokine

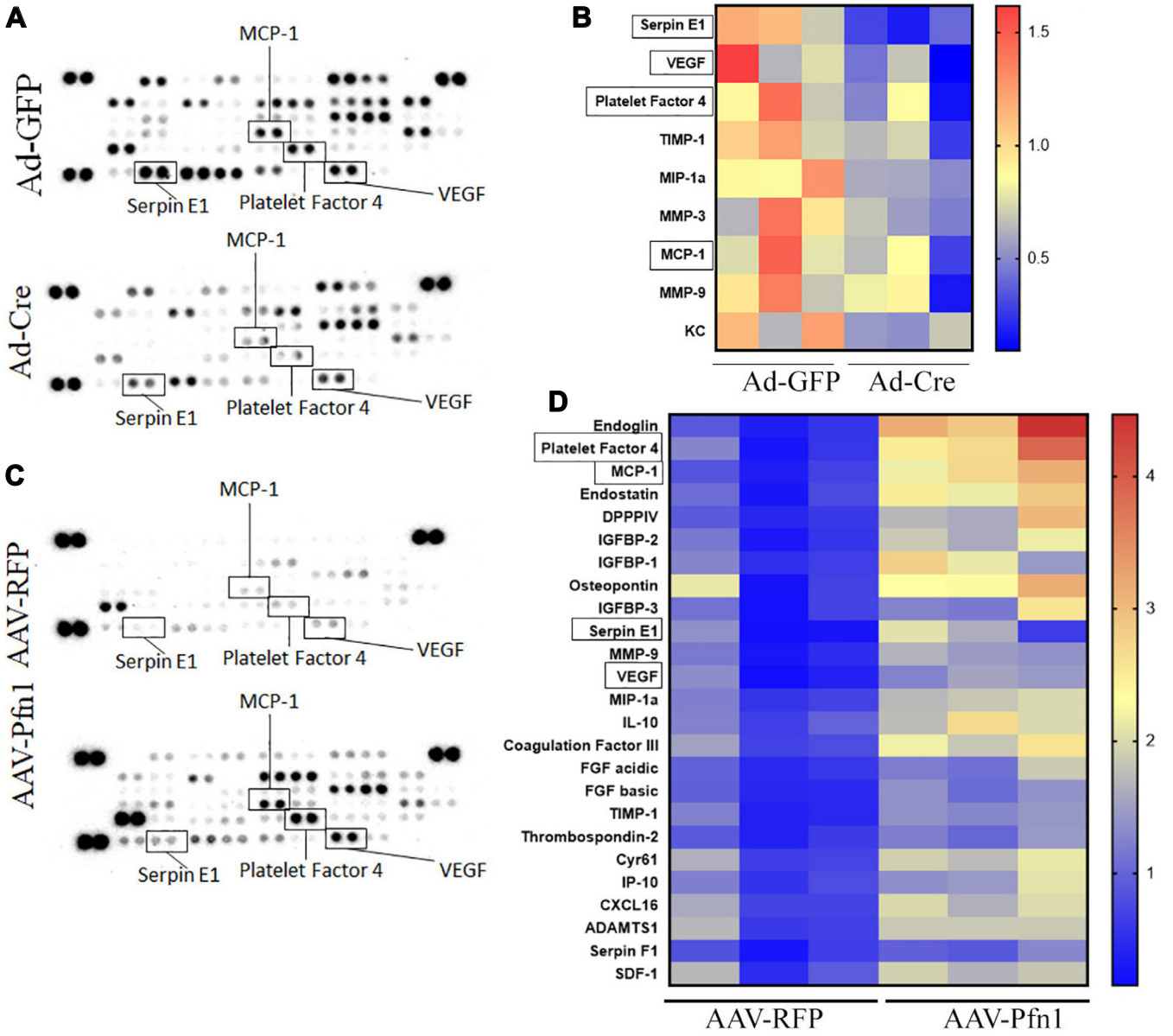

Figure 6. Effect of kidney-localized endothelial Pfn1 perturbation on tumor abundance of angiogenesis-related factors in mouse model of RCC. *A–D*, representative images of dot blot arrays (*A*), probing the expression of various angiogenesis-regulatory factors in RENCA tumor lysates from kidney-localized gene deletion (Ad-GFP *versus* Ad-Cre) and overexpression (AAV-RFP *versus* AAV-Pfn1) experiments (*C*). The data are summarized in the form of heat plots (*B* and *D*) with factors displayed in the decreasing order of fold change from the *top* to the *bottom* (N = 3 tumors/group). Fold change cut-off chosen were 1.5 and 2 for gene deletion and overexpression studies, respectively. Factors outlined by rectangles (VEGF, SerpinE1, MCP1/CCL2, and PF4) exhibited opposite directional changes in deletion *versus* overexpression experiments. AAV, adeno-associated virus; PF4, platelet factor 4; RCC, renal cell carcinoma.

belonging to IL6 family) that were not corroborated by RNA-seq analyses. We next performed Ingenuity Pathway Analysis (IPA) of DEGs to determine which biological pathways are most heavily impacted by loss of endothelial Pfn1. Although glycolysis ranked the top most pathway inhibited when endothelial Pfn1 expression is disrupted, the vast majority of top pathways affected by loss of endothelial Pfn1 were found to be related to immune regulation. These include upregulation of several T-cell–related pathways and downregulation of MSP-RON (macrophage-stimulating protein/recepteur d'origine Nantais, a major signaling pathway for stimulating macrophage chemotaxis) and immune checkpoint (PD1/PDL1 and CTLA4) signaling (Fig. 7*C*). Gene set enrichment analysis of the DEGs also revealed that loss of endothelial Pfn1 led to negative gene set enrichment of immune response such as adaptive immune response, T-cell activation, and lymphocyte activation (Fig. S8). Accordingly, IPA showed that pro-inflammatory genes are predominantly upregulated upon loss of endothelial Pfn1 expression (Fig. S9). These results, taken together our mouse model and clinical correlation findings, are consistent with a model that endothelial Pfn1 promotes an immunosuppressive TME in RCC.

To further explore the candidate gene regulatory networks that are perturbed by loss of endothelial Pfn1, we next performed upstream regulator analysis of EC Pfn1-responsive genes in IPA. These analyses predicted inhibition and

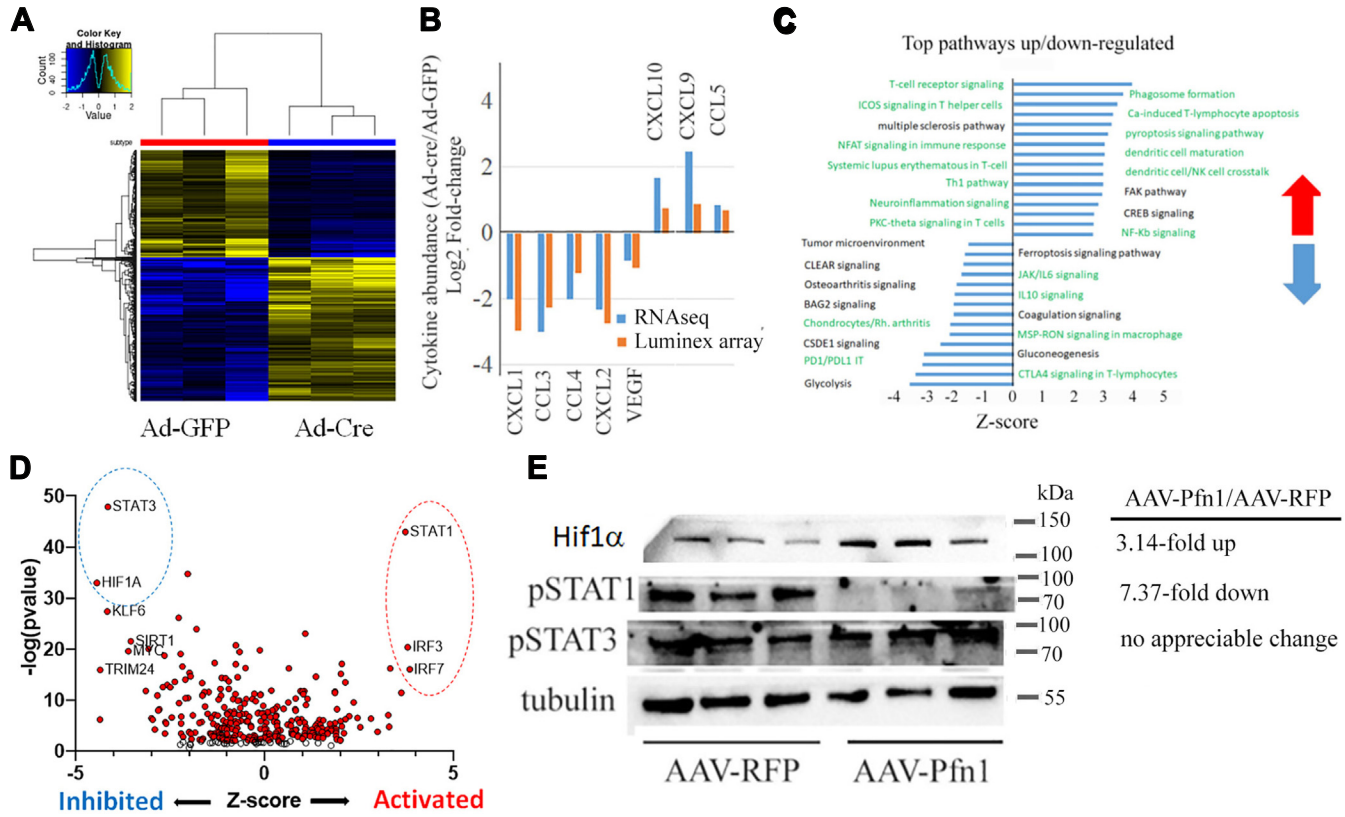

Figure 7. Impact of endothelial Pfn1 depletion on tumor abundance of immunomodulatory cytokines/chemokines and tumor transcriptome in mouse model of RCC. *A*, heat plot showing differentially expressed genes between Ad-GFP– and Ad-Cre–administered RENCA tumors (genes color coded by *blue* and *yellow* denotes transcriptionally downregulated and upregulated genes in Ad-Cre– relative to Ad-GFP–administered tumors; n = 3 tumors/per group). Differentially expressed genes were selected based on a mean fold cut-off change and false discovery rate set to 1.5 and 0.05, respectively. *B*, mean fold changes in tumor abundance of immunoregulatory cytokine and chemokine abundance based on RNAseq and luminex-based cytokine array analyses of tumor lysates (n = 3 tumors for each group with each sample analyzed in duplicate for cytokine array). Note that only those factors which were consistently elevated or downregulated by at least 1.5 fold in all three samples (analyzed in duplicate) of the experimental group relative to control in luminex assays and orthogonally validated by RNAseq are regarded as differentially abundant factors and displayed here. *C*, Ingenuity Pathway Analysis (IPA)-based prediction of top pathways upregulated and downregulated in Ad-Cre– relative to Ad-GFP–administered tumors selected based on the Z-score —a total of 16 and 15 pathways are shown for upregulated and downregulated pathways, respectively, with pathways annotated by *green* denoting those related to immune cell regulation. *D*, a volcano plot (*p*-value *versus* Z score) displaying IPA-predicted activated and inhibited transcription factors in Ad-Cre– *versus* Ad-GFP–administered tumors. Top IPA-predicted activated and inhibited transcription factors (based on the absolute Z score and negative log *p*-value) are outlined by *red* and *blue ovals*, respectively. *E*, immunoblots showing relative changes in HIF1α, STAT1, and STAT3 phosphorylation in AAV-Pfn1– relative to AAV-RFP–administered RENCA tumors (tubulin blot–loading control). Three tumors in each group are represented, and the fold change for any given protein displayed is the ratio of mean band intensity of AAV-Pfn1 to the AAV-RFP lanes following normalization to the loading control. AAV, adeno-associated virus; HIF, hypoxia-inducible factor; RCC, renal cell carcinoma.

activation of a wide range of transcription factors as shown in the form of a volcano plot (Fig. 7*D*; a complete list is provided in Table S2) that have well-known roles in regulating tumorigenesis, angiogenesis, metabolism, and immune regulation (*e.g.*, HIF1α, STAT1, STAT3, and interferon-regulatory factors (IRFs)). Interestingly, IRFs (IRF3 and IRF7) and STAT1, both of which are known to promote M1-like macrophage differentiation linked to effective antitumor immune responses (28), are the top three transcription factors that were predicted to be activated upon loss of endothelial Pfn1 (Fig. 7*D*). Conversely, HIF1α (a major driver of VEGF transcription and disease progression in ccRCC) activity was predicted to be downregulated when Pfn1 expression is disrupted in EC. Consistent with RNA-seq predicted analyses from knockout studies, immunoblot analyses of tumors from overexpression studies demonstrated HIF1α upregulation and a striking downregulation of STAT1 phosphorylation in AAV-Pfn1–administered tumors relative to control AAV-RFP–administered tumors (Fig. 7*E*). Based on all of our mouse model data and clinical correlation findings, we propose a schematic model of how either loss or elevated level of endothelial Pfn1 impacts tumor-promoting microenvironment in RCC (Fig. 8).

Loss of VHL does not negate endothelial Pfn1's requirement for tumorigenic ability of RCC cells

Although RENCA cell line does not exhibit the typical oncogenetic developmental pathways (deletion and/or mutation of *VHL*, *PBRM1*, *BAP1*, *SETD2*) found in human ccRCC, previous studies have shown that VHL deletion alone in RENCA cells leads to upregulation of many genes and induces histological features in tumors that are associated with aggressive ccRCC in humans (29, 30). Therefore, we performed an exploratory study with iVDR (inducible VHL-deleted RENCA), a subline of RENCA we engineered for

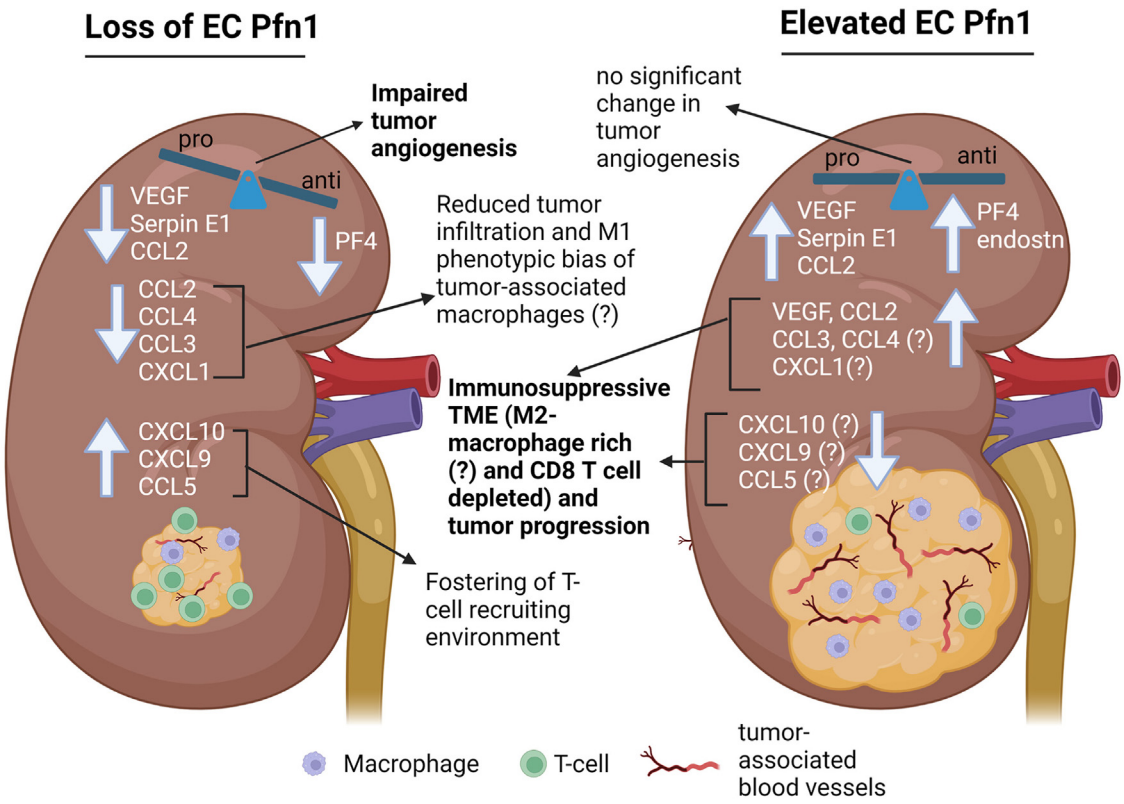

Figure 8. A graphical summary of how RCC tumor microenvironment is impacted by either loss of or elevated endothelial Pfn1. The key changes in angiogenesis- and immuno-regulatory factors and their consequences are shown in each case (endost, endostatin). Postulates or factors that are yet to be verified experimentally are denoted by *question marks*. RCC, renal cell carcinoma.

CRISPR/Cas9-mediated deletion of VHL under a doxycycline (DOX)-inducible Cas9 expression system (Fig. S10*A*). Inducible Cas9 expression system enabled us to turn off Cas9 expression permanently by DOX withdrawal after VHL was deleted to avoid any unwanted immune reaction against Cas9-xenoantigen and tumor rejection *in vivo*. Similar to our results seen for VHL+ RENCA cells, tumorigenic ability of iVDR cells was also dramatically hindered by loss of Pfn1 expression in vascular endothelial cells *in vivo* (Fig. S10*B*). Collectively, these results demonstrate that endothelial Pfn1 is a critical requirement for tumorigenesis of RCC cells regardless of its VHL expression status.

Discussion

In the present study, we report several novel findings. First, while we and others previously correlated higher Pfn1 expression with advanced disease feature and poor clinical outcome of RCC patients (8–12), a causal link between Pfn1 dysregulation and RCC aggressiveness in an *in vivo* setting was not established. Based on our previous discovery of predominance of Pfn1 overexpression in tumor-associated vascular EC rather than in tumor cells in ccRCC (8), this study for the first time utilizes kidney-localized knockout and overexpression of endothelial Pfn1 to demonstrate a critical requirement for vascular endothelial Pfn1 for tumorigenicity in orthotopic tumor models of RCC. Furthermore, in a delayed global endothelial Pfn1 knockout setting, we demonstrate that endothelial Pfn1 is also vitally important for progressive growth of pre-established kidney tumors. Second, we establish Pfn1's indispensable role in tumor angiogenesis and identify Pfn1-dependent changes in several prominent pro- and anti-angiogenic factors in RCC TME *in vivo*. Third, we undertook a comprehensive strategy combining mouse model data with analyses of multiplexed quantitative IHC and transcriptome analyses of clinical samples of RCC for the first time to define a novel role of endothelial Pfn1 in fostering an immunosuppressive TME in RCC with mechanistic insights.

Reduced tumor angiogenesis in the setting of kidney-localized deletion of endothelial Pfn1 as well as massive necrosis of pre-established tumor following widespread deletion of endothelial Pfn1 clearly suggest that defect in tumorigenicity and progressive growth of RCC cells in endothelial Pfn1-deficient condition primarily results from lack of adequate blood supply in the tumor (as schematized in Fig. 8). Our findings are consistent with previously reported reduced tumor angiogenesis in glioblastoma when endothelial Pfn1's ability to undergo phosphorylation on its Y129 residue (a posttranslational modification that promotes Pfn1's interaction with VHL relieving VHL–HIF1 interaction, HIF stabilization, and upregulation of pro-angiogenic factors including VEGF) is ablated (22). Our experimental data also support endothelial Pfn1's ability to enhance HIF1α (at protein level) and VEGF (at mRNA and protein levels) in RCC TME. In fact, HIF1 is one of the top transcription factors that is predicted to be inactivated by loss of endothelial Pfn1 as per our IPA

analyses. Therefore, suppression of HIF1–VEGF signaling axis could be one of the key mechanisms underlying defect in tumor angiogenesis in the setting of loss of endothelial Pfn1.

Our studies also uncovered several additional angiogenesis-regulatory factors (both pro- and anti-angiogenic) besides VEGF that are appreciably impacted by endothelial Pfn1 perturbation *in vivo*. Pro-angiogenic factors that are positively influenced by endothelial Pfn1 (based on both KO and overexpression studies) include SERPIN family E member 1 (SERPINE1), CCL2/MCP1, CCL3/MIP1α, and several MMPs (MMP3 and MMP9). In fact, SERPINE1 was most robustly downregulated (even more than VEGF) when Pfn1 expression was disrupted in EC. SERPIN1 gene encodes plasminogen activator inhibitor 1 that restricts the activity of the Urokinase-type plasminogen activator (31). Although Urokinase-type plasminogen activator's action leads to extracellular matrix proteolysis and activation of MMPs and latent growth factors promoting angiogenesis (32), paradoxically SERPINE1 has pro-angiogenic and protumorigenic functions (33–35). With regard to angiogenesis inhibition, although PF4 was the only anti-angiogenic factor (36) that we were able to link to Pfn1 perturbation in both knockout and overexpression settings, we found endostatin, a matricellular protein with potent anti-angiogenic action (37), to be also heavily upregulated in the TME when Pfn1 was overexpressed in EC. Our observation of endothelial Pfn1's ability to simultaneously promote the abundance of pro-angiogenic factors (several besides VEGF) and anti-angiogenic factors in the TME not only suggests that Pfn1 could potentially also promote angiogenesis in a VEGF-independent manner but may also explain why Pfn1 overexpression in EC unexpectedly did not further augment angiogenesis. Since both endostatin and PF4 are known to block VEGF's binding to its receptor (38), it is possible that pro-angiogenic benefit of VEGF upregulation in endothelial Pfn1 overexpression setting is nullified by VEGF–VEGFR interaction blockade by increased extracellular presence of these factors in Pfn1 overexpression setting (as schematized in Fig. 8).

Given that endothelial Pfn1 overexpression leads to macrophage enrichment and attenuation of tumor infiltration by T cells (including CD8+ sub-population) of TME and accelerates tumor progression without affecting tumor angiogenesis, we postulate that Pfn1 elevation promotes tumor progressing primarily through fostering an immunosuppressive TME (as schematized in Fig. 8). This postulate is at least peripherally supported by two sets of observations. First, our cytokine/chemokine profiling data in Pfn1 knockout setting are consistent with a scenario that endothelial Pfn1's presence stimulates immunomodulatory factors that polarize macrophages into tumor-promoting, anti-inflammatory M2-like phenotype (*e.g.*, CXCL2, CXCL1, CCL2, CCL3, CCL4, VEGF—Pfn1's positive effects on CCL2, CCL3, and VEGF were also verified in the overexpression setting) and, concomitantly, reduces effector T cell–recruiting factors (CXCL10, CXCL9, and CCL5) abundance in the RCC TME. Second, our RNA-seq data also predicted IRFs (IRF3 and IRF7) and STAT1 (both known to promote M1-like differentiation of macrophages and antitumor immune response (28)) to be among the top three activated transcription factors in RCC tumors when endothelial Pfn1 expression is disrupted. This was further validated by reduced STAT1 phosphorylation in RCC tumors with endothelial-overexpressed Pfn1.

How might endothelial Pfn1 elevation promote an immunosuppressive TME? We can speculate several testable hypotheses for future investigations. First, our IPA predicted that endothelial Pfn1 loss leads to downregulation of MSP-RON (RON, the receptor for MSP), an HGF-like receptor tyrosine kinase signaling pathway. MSP-RON signaling promotes tumor infiltration of macrophages, polarize macrophages into an M2-like phenotype, and suppresses T cell–mediated antitumor response through inhibition of Toll-like receptor (TLR) signaling pathway (39). MSP-RON signaling also directly promotes cancer cell proliferation in a tumor-intrinsic manner (40). Downstream signatures of MSP-RON signaling such as increased production of CCL2 and CXCL2 and suppression of IRF (activated by TLR signaling) and STAT1 activity (also activated downstream of and an important player in TLR signaling) resonate with our experimental observation of downregulation of both CCL2 and CXCL2 and predicted activated IRF and STAT1 in the endothelial Pfn1-depleted tumors. Second, SERPINE1, a gene that we found to be significantly altered in expression upon endothelial Pfn1 perturbation and was previously shown to correlate with tumor infiltration of macrophages and CD8+ T cells in adenocarcinoma (41), could also be a potential mediator of immunomodulatory activity of endothelial Pfn1. Third, we previously showed that Pfn1 is also secreted in the extracellular milieu by various cells (EC, tumor cells) and that extracellular Pfn1 has biological activity (8). Given previous experimental evidence for intracellular Pfn1's ability to inhibit migration and cytotoxic activity of T cells (42), endothelial Pfn1 overexpression can increase extracellular Pfn1 content in the TME to negatively impact T cell migration.

Although the present study was predominantly conducted with VHL+ RENCA cells for proof-of-concept, our exploratory findings demonstrating endothelial Pfn1 dependence for tumorigenicity of VHL-null iVDR cells indicates that endothelial Pfn1's requirement for disease progression also translates to clear cell pathology. VHL deletion in cancer cells should, in principle, dramatically elevate HIF-mediated upregulation of pro-angiogenic factors including VEGF and is unlikely to set VEGF abundance in the TME as a limiting factor. Therefore, we speculate that Pfn1-dependent changes in endothelial VEGF expression *per se* may not be the dominant mechanism underlying the defect in tumorigenicity of iVDR cells in endothelial Pfn1-deficient condition. Glycolysis is the primary energy-generating mechanism of vascular EC and is critically important for rapid EC migration, proliferation, and angiogenesis in physiological and pathological settings (43). Given that glycolysis ranks the top downregulated pathway in endothelial Pfn1 KO RENCA tumors (consistent with downregulation of HIF activity), impaired glycolysis may be one of the major mechanisms contributing to impaired tumorigenicity of VHL-null RCC cells in endothelial Pfn1-deficient condition, a hypothesis that can be tested in future studies.

In conclusion, this study demonstrates that endothelial Pfn1 plays a critical role in shaping vascular and immunogenic aspect of TME, tumorigenesis, and tumor progression in RCC. These findings, taken together previously demonstrated tumor-intrinsic role of Pfn1 in promoting RCC cell aggressiveness *in vitro* and strong clinical association between higher Pfn1 expression and poor clinical outcome of ccRCC patients (8–12), provide a conceptual basis for targeting Pfn1 for therapeutic benefit in kidney cancer.

Experimental procedures

Cell culture and viral transduction

RENCA cells (CRL-2947, ATCC) were cultured in RPMI media supplemented with 10% (v/v) fetal bovine serum and antibiotics (100 U/ml penicillin and 100 μg/ml streptomycin). GFP-Luciferase reporter was introduced into RENCA cells by infecting them with lentivirus containing firefly luciferase and EGFP following manufacturer's protocol (79980-G, BPS Bioscience). To generate inducible VHL-deleted RENCA (IVDR) cells, we utilized Dharmacon Edit-R CRISPR-Cas9 gene engineering system to first stably express DOX-inducible Cas9 (VCAS11227, Dharmacon). After selecting for Cas9-expressing RENCA cells, we then introduced VHL sgRNA following Dharmacon's Edit-R protocol (VSGM10144-246741600, Dharmacon, target - GCCCGGTGGTAAGATCGGGT). VHL-null variants of RENCA (iVdR) were clonally selected from the initial transduced pool.

Isolation and immortalization of mouse kidney Pfn1-floxed EC

Kidneys harvested from adult $Pfn1^{flox/flox:}$ FVB mice were digested by collagenase. Single cell isolates from collagenase digests were labeled with MACS mouse CD31 magnetic beads (130-097-418, Miltenyi Biotec) and then isolated using magnetic LS columns following manufacturer's recommended protocol. CD31-MACS sorted cells were then plated on top of collagen-1 (50 μg/ml)–coated tissue culture dish in complete EC medium (M1168, Cell Biologics Inc) and grown before infecting with hTERT (human telomerase reverse transcriptase)-encoding lentivirus (LP726-025, GeneCopoeia; MOI = 5) to generate an immortalized mouse kidney EC line with floxed Pfn1 (denoted as $MEC^{Pfn1\text{-}fl}$). $MEC^{Pfn1\text{-}fl}$ cells were infected with Ad-CDH5-Cre (or Ad-GFP as control; MOI = 10) and AAV1-CDH5-Pfn1 (or AAV1-RFP as control; MOI = 100) before extracting cell lysates for immunoblot-based confirmation of depletion and overexpression of Pfn1, respectively.

Protein extraction and immunoblotting

Cell lysates were prepared by a modified RIPA buffer (25 mM Tris–HCL: pH 7.5, 150 mM NaCl, 1% (v/v) NP-40, 5% (v/v) glycerol), 1 mM EDTA, 50 mM NaF, 1 mM sodium pervanadate, and protease inhibitors supplemented with 6x sample buffer diluted to 1× with the final SDS concentration in the lysis buffer equivalent to 2%. Conditions for the various antibodies for immunoblotting purpose were as follows: monoclonal Cas9 (CST, 14697; 1:1000), monoclonal Tubulin (Sigma, T9026, 1:3000), polyclonal VHL (Thermo Fisher Scientific, PA5-87428; 1:1000), monoclonal Hif1α (Thermo Fisher Scientific, NB100105SS, 1:1000), polyclonal Hif2α (Thermo Fisher Scientific, NB100122SS, 1:1000), monoclonal pSTAT1 (CST, 9167, 1:1000), monoclonal pSTAT3 (CST, 9145, 1:1000), and monoclonal Pfn1 (Abcam, AB124904). Chemiluminescence-based detection kit was used to reveal bands in immunoblots, and band intensity quantification was performed within the linear range of intensity values.

Animal studies

All animal experiments were conducted in compliance with an approved IACUC protocol, according to University of Pittsburgh Division of Laboratory Animal Resources guidelines. Generation of $Pfn1^{flox/flox:}$CDH5-Cre-ERT2 mice was previously described (17). To achieve widespread endothelial Pfn1 gene knockout, adult $Pfn1^{flox/flox:}$ CDH5-Cre-ERT2 mice were subjected to daily intraperitoneal injection of tamoxifen (75 mg/kg mouse body weight) for five consecutive days.

Matrigel plug angiogenesis assay

Six-week-old Balb/c mice ($Pfn^{+/+}$ or $Pfn1^{-/-(EC)}$) were anesthetized and injected subcutaneously at the flanks with 0.5 ml of reduced growth factor Matrigel (R&D Systems, 3533-010-02) with 2×10^5 RENCA cells supplemented with 500 ng of basic fibroblast growth factor. Number of functional blood vessels (red blood cell–positive) were scored from three histological sections at multiple fields per animal.

Orthotopic tumor model

Five- to six-week-old mice were anesthetized with a vaporizer using 4% isoflurane and maintained at 2% isoflurane on a heating plate kept at 38 °C while undergoing surgery. The right flank of mouse was shaved and disinfected before making a superficial incision in the skin without damaging the peritoneal wall to reveal the right kidney. The right kidney was pushed against the peritoneal wall, and RCC cells (25×10^4 and 15×10^4 cells for endothelial Pfn1 KO and overexpression experiments, respectively), suspended in 100 μl PBS, were injected into the kidney. For kidney-localized deletion of endothelial Pfn1, 2×10^{10} viral particles of either Ad-GFP or Ad-CDH5-Cre were co-injected with tumor cells. For kidney-localized overexpression of Pfn1, 2×10^{11} viral particles of either AAV1-RFP or AAV1-CDH5-Pfn1 (co-expresses mCherry reporter) were co-injected with tumor cells. For progressive growth studies, tamoxifen-mediated deletion of endothelial Pfn1 was initiated after allowing tumors to form for 7 days. Bioluminescence images of tumor-bearing mice were acquired with IVIS Spectrum 15 min after intraperitoneal injection of D-luciferin (50 mg/kg) and were analyzed by Living Image 4.3 software (PerkinElmer, https://www.perkinelmer.com/product/spectrum-200-living-image-v4series-1-128113). At necropsy, kidneys were excised for assessment of tumor burden (weight of tumor-bearing kidney relative to that of uninvolved kidney). H&E staining of kidney and lung sections (utilizing the service provided by the University of Pittsburgh McGowan Institute of Regenerative Medicine histology core) were performed for orthogonal

confirmation of kidney tumor and lung metastases on 4% paraformaldehyde-fixed tissue samples.

RNA sequencing

Total RNA was isolated from tumor tissue using RNeasy Mini Plus Kit (Qiagen) following manufacturer's protocol. Samples were submitted to the University of Pittsburgh HSCRF Genomics Research Core for RNA-seq. The Core determined the quality and quantity of the RNA (Bioanalyzer), prepared multiplexed paired-end libraries (Illumina TruSeq), and sequenced the samples on an Illumina NextSeq to a minimum of 22 million reads per sample. Quality of sequencing reads was determined with FastQC before transcripts from the Ensembl v.93 transcriptome (hg38) were quantified with Salmon v0.14.0. Gene-level expression was calculated using tximport v.1.12.0, differential gene expression was calculated with DESeq2 v.1.24.0, and BiomaRt v.2.46.0 was used to annotate gene names. Genes with a minimum expression greater than 1 transcripts per million in either control or experimental group, an adjusted *p*-value less than 0.05, and a shrunken fold change less than or greater than 1.5 were considered differentially expressed. IPA was performed on DEGs according to protocol with z-scores and *p*-values extracted for specific diseases, biological functions, and canonical pathways and plotted with ggplot2 v.3.3.2 in R. An upstream regulator analysis was also performed within IPA with all DEGs as input. All scripts are available upon request.

Cytokine analyses

Tumor tissue was probed for cytokine/chemokine expression levels by Luminex analysis by service provided by Eve Technologies using MD31 (32-analyte murine discovery panel) panel. For cytokine analyses, analyte values were normalized to the average value of control animals within litters.

Angiogenesis array

Tumor lysates (30 mg total protein prepared in modified RIPA buffer) were profiled for expressions of a panel of 53 pro- and anti-angiogenic signaling factors using Proteome Profiler Mouse Angiogenesis Array (ARY015, R&D Systems) as per manufacturer's instruction.

Renal cell carcinoma tissue microarray

The RCC TMAs (comprising a total of 191 patient tumors with predominantly clear cell histology) were obtained from the tissue bank of the National Center for Tumor Diseases, University of Heidelberg (52) and used in accordance with the regulations of the tissue bank as well as under approval of the Ethics Committee of the University of Heidelberg School of Medicine, abiding by the declaration of Helsinki Principle. Multiplexed immunostaining of TMA was performed using Akoya Biosciences manufacturer's protocol with the following antibodies: Pfn1: 1:800 (Abcam, Cat# ab124904), CD8: 1:150 (Biocare Medical, Cat# ACI 3160A), CD68: 1:800 (Cell Signaling, Cat# 76437S), Pan-CK: 1:100 (Santa Cruz, Cat# sc-81714), FOXP3: 1:150 (CST, Cat# 98377), and CD31: 1:150. (Biocare Medical, Cat# CM131A) and DAPI (AkoyaBio kit). TMA spots were imaged using Vectra Polaris and analyzed using "inForm Tissue Analysis Software" and "phenoptr" which is an R script from Akoya (open source, https://www.akoyabio.com/phenoimager/software/inform-tissue-finder/) that consolidates/analyzes output tables generated in inForm.

Immunohistochemistry

Tissue sections were deparaffinized and rehydrated before incubating overnight with the primary antibodies followed by secondary antibodies. The primary antibodies used were as follows: anti-CD31 antibody (77699, CST, 1:100 or NB1001642, Novus Biologicals, 1:100), anti-CD3 (78588, CST, 1:100), anti-CD8 antibody (98941, CST, 1:100), anti-F4/80 antibody (70076, CST, 1:100), and anti-Pfn1 antibody (AB124904, Abcam, 1:100). For immunodetection of primary antibodies, secondary antibodies used were as follows: FITC-conjugated anti-rabbit antibody (111-095-003, Jackson ImmunoResearch, 1:100), FITC-conjugated anti-rat antibody (50-194-1889, Jackson ImmunoResearch, 1:100), or TRITC-conjugated anti-rabbit antibody (111-025-003, Jackson ImmunoResearch, 1:100). The slides were counterstained with DAPI in the mounting media (P36935, Thermo Fisher Scientific).

Immune deconvolution analyses

The TCGA ccRCC raw count matrix was downloaded from Xena platform GDC hub (43) and normalized using R package DESeq2 (ver. 1.38.3) (44). We obtained ccRCC scRNAseq (n = 7) and cell type annotations from GSE159115) (27) and analyzed using R package Seurat (ver. 4.3.0) (45). SCTransform was applied to each Seurat object for data normalization and transformation. All the Seurat objects were merged, SCTransform was applied regressing out mitochondrial read percentage, and the data integration was performed using R package Harmony (ver. 1.0) (46). We calculated cell type fraction across seven patients and then determined and calculated the Spearman correlation between mean Pfn1 expression and cell type fraction across patients for each cell type subset. Using the scRNA-seq data, we defined a signature matrix of genes that differentiate each cell type of interest. We applied CIBERSORTx (47) to estimate the proportion of different cell types for each tumor sample in the TCGA ccRCC RNA-seq dataset (n = 535). We ran the CIBESORTx algorithm with default settings, excluding quantile normalization, for 100 permutations with our reference signature matrix and estimated the abundance of immune and stromal cell types. We obtained the relative proportions of 12 subsets of tumor-infiltrating immune cells in each sample with p-value <0.01 measuring the confidence of the results for the deconvolution. We calculated the Spearman correlation between estimated cell type fractions and mRNA expression of Pfn1 and its closest isoform Pfn2 in TCGA ccRCC tumors.

Cellular neighborhood analysis

For each TMA, we constructed a neighborhood graph connecting all cells that are within 100 μm Euclidean distance

of each other. For each cell, we summed the number of neighboring cells of each cell type, resulting in a 5-length vector. We performed cellular neighborhood (CN) analysis in a similar way as previously described (48). The neighborhood vector for each cell was normalized to have sum of one so that the values correspond the proportion of each cell type within proximity to the cell. The proportions for each cell type were normalized to have mean zero and SD of 1 before the neighborhood vectors were clustered using Python's scikit-learn (v 1.1.3) implementation of MiniBatchKMeans with the number of clusters set as 5. Each of these five clusters were termed as CNs, and each cell was assigned to the neighborhood based on its neighborhood vector. The cluster for each CN has a 'centroid' vector, which is interpreted as the typical proportion of each cell type for the CN and used to give qualitative descriptions to each CN. For the set of all CK+ cells, we use one-way ANOVA and post hoc Tukey honestly significant difference to assess the difference in log PFN1 expression for cells assigned to each neighborhood. The process was repeated for CD31+ cells. One-way ANOVA and post hoc Tukey honestly significant difference tests were performed using the statsmodels python package (v 0.13.2).

mRNA extraction and RT-PCR

Total RNA was extracted from cultured cells using RNeasy mini kit (Qiagen, 74104) according to manufacturer's instructions. Complementary DNA was synthesized from 1 μg of RNA using the Quantitect reverse transcription kit (Qiagen, 205311) following the manufacturer's instructions. RT-PCR of target genes was performed with 50 ng of complementary DNA. The primer sequences for mCherry RT-PCR were 5′-GCATGGACGAGCTGTACAAG-3′ (sense) and 5′-GCATGAACTCCTTGATGATG-3′ (antisense). The primer sequences for Cre RT-PCR were 5′-GCCTGCATTACCGGTCGATGCAACGA-3′ (sense) and 5′-GTGGCAGATGGCGCGGCAACACC-3′ (antisense). The PCR cycling conditions were 95 °C (30 s), 55 °C (30 s), and 72 °C (1 min) for a total of 40 cycles.

Statistics

Statistical tests were performed with either one-way ANOVA followed by Tukey's post hoc test or nonparametric Mann–Whitney test when appropriate. Kruskal–Wallis test was used for ranked analysis of small samples. Differences exhibiting $p < 0.05$ were considered as statistically significant.

Data availability

All data are included as either main figures or supplemental information.

Supporting information—This article contains supporting information.

Acknowledgment—The authors wish to thank Jessica Kunkel for assisting with quantification of matrigel plug angiogenesis data.

Author contributions—D. G., A. D., A. A., M. J., and S. L. investigation; D. G., A. D., M. J., A. S., P. C. L., D. B., and H. U. O. formal analysis; D. G. and P. R. conceptualization; D. G., A. S., S. L., and P. R. writing–original draft; D. G., H. U. O., and P. R. funding acquisition; P. C. L. and H. U. O. writing–review and editing; S. D. resources; P. R. and H. U. O. supervision.

Funding and additional information—D. G. was supported by a National Cancer Center fellowship, NCI K99-CA267180 and T32-HL129964. A. A. G. was supported by National Institutes of Health fellowship, 5F31HL160188. A. S. was supported by National Library of Medicine Training grant [T15 LM007059-24]. H. U. O. was supported by the NIGMS R35GM146989 and NCI R00CA207871 grants. P. R. was supported by Department of Defense (W81XWH-19-1-0768) and NCI R01CA248873 grants. The content is solely the responsibility of the authors and does not necessarily represent the official views of the National Institutes of Health.

Conflict of interest—The authors declare that they have no conflict of interest with the contents of this article.

Abbreviations—The abbreviations used are: AAV, adeno-associated virus; BLI, bioluminescence imaging; ccRCC, clear cell RCC; CK, cytokeratin; CN, cellular neighborhood; DEG, differentially expressed gene; DOX, doxycycline; EC, endothelial cell; HIF, hypoxia inducible factor; IHC, immunohistochemistry; IPA, Ingenuity Pathway Analysis; IRF, interferon-regulatory factor; iVDR, inducible VHL-deleted RENCA; MMP, matrix metalloproteinase; MSP-RON, macrophage-stimulating protein/recepteur d'origine Nantais; PF4, platelet factor 4; Pfn1, Profilin-1; RCC, renal cell carcinoma; RT-PCR, reverse transcription-polymerase chain reaction; SERPINE1, SERPIN family E member 1; TCGA, The Cancer Genome Atlas; TLR, Toll-like receptor; TMA, tissue microarray; TME, tumor microenvironment; VEGF, vascular endothelial growth factor; VHL, Von-Hippel Lindau.

References

1. Siegel, R. L., Miller, K. D., Wagle, N. S., and Jemal, A. (2023) Cancer statistics, 2023. *CA Cancer J. Clin.* **73**, 17–48
2. Gupta, K., Miller, J. D., Li, J. Z., Russell, M. W., and Charbonneau, C. (2008) Epidemiologic and socioeconomic burden of metastatic renal cell carcinoma (mRCC): a literature review. *Cancer Treat. Rev.* **34**, 193–205
3. Cindolo, L., Patard, J. J., Chiodini, P., Schips, L., Ficarra, V., Tostain, J., *et al.* (2005) Comparison of predictive accuracy of four prognostic models for nonmetastatic renal cell carcinoma after nephrectomy: a multicenter European study. *Cancer* **104**, 1362–1371
4. Shigeta, K., Datta, M., Hato, T., Kitahara, S., Chen, I. X., Matsui, A., *et al.* (2020) Dual programmed death receptor-1 and vascular endothelial growth factor receptor-2 blockade promotes vascular normalization and enhances antitumor immune responses in hepatocellular carcinoma. *Hepatology* **71**, 1247–1261
5. Goel, S., Duda, D. G., Xu, L., Munn, L. L., Boucher, Y., Fukumura, D., *et al.* (2011) Normalization of the vasculature for treatment of cancer and other diseases. *Physiol. Rev.* **91**, 1071–1121
6. Bergers, G., and Hanahan, D. (2008) Modes of resistance to anti-angiogenic therapy. *Nat. Rev. Cancer* **8**, 592–603
7. Welti, J., Loges, S., Dimmeler, S., and Carmeliet, P. (2013) Recent molecular discoveries in angiogenesis and antiangiogenic therapies in cancer. *J. Clin. Invest.* **123**, 3190–3200
8. Allen, A., Gau, D., Francoeur, P., Sturm, J., Wang, Y., Martin, R., *et al.* (2020) Actin-binding protein profilin1 promotes aggressiveness of clear-cell renal cell carcinoma cells. *J. Biol. Chem.* **295**, 15636–15649
9. Karamchandani, J. R., Gabril, M. Y., Ibrahim, R., Scorilas, A., Filter, E., Finelli, A., *et al.* (2015) Profilin-1 expression is associated with high grade

and stage and decreased disease-free survival in renal cell carcinoma. *Hum. Pathol.* **46**, 673–680
10. Masui, O., White, N. M., DeSouza, L. V., Krakovska, O., Matta, A., Metias, S., *et al.* (2013) Quantitative proteomic analysis in metastatic renal cell carcinoma reveals a unique set of proteins with potential prognostic significance. *Mol. Cell. Proteomics* **12**, 132–144
11. Minamida, S., Iwamura, M., Kodera, Y., Kawashima, Y., Ikeda, M., Okusa, H., *et al.* (2011) Profilin 1 overexpression in renal cell carcinoma. *Int. J. Urol.* **18**, 63–71
12. Neely, B. A., Wilkins, C. E., Marlow, L. A., Malyarenko, D., Kim, Y., Ignatchenko, A., *et al.* (2016) Proteotranscriptomic analysis reveals stage specific changes in the molecular landscape of clear-cell renal cell carcinoma. *PLoS One* **11**, e0154074
13. Klatt, M. G., Kowalewski, D. J., Schuster, H., Di Marco, M., Hennenlotter, J., Stenzl, A., *et al.* (2016) Carcinogenesis of renal cell carcinoma reflected in HLA ligands: a novel approach for synergistic peptide vaccination design. *Oncoimmunology* **5**, e1204504
14. Stickel, J. S., Weinzierl, A. O., Hillen, N., Drews, O., Schuler, M. M., Hennenlotter, J., *et al.* (2009) HLA ligand profiles of primary renal cell carcinoma maintained in metastases. *Cancer Immunol. Immunother.* **58**, 1407–1417
15. Gau, D., Lewis, T., McDermott, L., Wipf, P., Koes, D., and Roy, P. (2018) Structure-based virtual screening identifies a small-molecule inhibitor of the profilin 1-actin interaction. *J. Biol. Chem.* **293**, 2606–2616
16. Gau, D., Veon, W., Capasso, T. L., Bottcher, R., Shroff, S., Roman, B. L., *et al.* (2017) Pharmacological intervention of MKL/SRF signaling by CCG-1423 impedes endothelial cell migration and angiogenesis. *Angiogenesis* **20**, 663–672
17. Gau, D., Vignaud, L., Allen, A., Guo, Z., Sahel, J., Boone, D., *et al.* (2020) Disruption of profilin1 function suppresses developmental and pathological retinal neovascularization. *J. Biol. Chem.* **295**, 9618–9629
18. Gau, D., Vignaud, L., Francoeur, P., Koes, D., Guillonneau, X., and Roy, P. (2021) Inhibition of ocular neovascularization by novel anti-angiogenic compound. *Exp. Eye Res.* **213**, 108861
19. Ding, Z., Gau, D., Deasy, B., Wells, A., and Roy, P. (2009) Both actin and polyproline interactions of profilin-1 are required for migration, invasion and capillary morphogenesis of vascular endothelial cells. *Exp. Cell Res.* **315**, 2963–2973
20. Ding, Z., Lambrechts, A., Parepally, M., and Roy, P. (2006) Silencing profilin-1 inhibits endothelial cell proliferation, migration and cord morphogenesis. *J. Cell Sci.* **119**, 4127–4137
21. Fan, Y., Arif, A., Gong, Y., Jia, J., Eswarappa, S. M., Willard, B., *et al.* (2012) Stimulus-dependent phosphorylation of profilin-1 in angiogenesis. *Nat. Cell Biol.* **14**, 1046–1056
22. Fan, Y., Potdar, A. A., Gong, Y., Eswarappa, S. M., Donnola, S., Lathia, J. D., *et al.* (2014) Profilin-1 phosphorylation directs angiocrine expression and glioblastoma progression through HIF-1α accumulation. *Nat. Cell Biol.* **16**, 445–456
23. Sivaraj, K. K., Dharmalingam, B., Mohanakrishnan, V., Jeong, H. W., Kato, K., Schröder, S., *et al.* (2020) YAP1 and TAZ negatively control bone angiogenesis by limiting hypoxia-inducible factor signaling in endothelial cells. *Elife* **9**, e50770
24. Sivaraj, K. K., Majev, P. G., Jeong, H. W., Dharmalingam, B., Zeuschner, D., Schröder, S., *et al.* (2022) Mesenchymal stromal cell-derived septoclasts resorb cartilage during developmental ossification and fracture healing. *Nat. Commun.* **13**, 571
25. Stachler, M. D., and Bartlett, J. S. (2006) Mosaic vectors comprised of modified AAV1 capsid proteins for efficient vector purification and targeting to vascular endothelial cells. *Gene Ther.* **13**, 926–931
26. Wu, S. Y., Liao, P., Yan, L. Y., Zhao, Q. Y., Xie, Z. Y., Dong, J., *et al.* (2021) Correlation of MKI67 with prognosis, immune infiltration, and T cell exhaustion in hepatocellular carcinoma. *BMC Gastroenterol.* **21**, 416
27. Zhang, Y., Narayanan, S. P., Mannan, R., Raskind, G., Wang, X., Vats, P., *et al.* (2021) Single-cell analyses of renal cell cancers reveal insights into tumor microenvironment, cell of origin, and therapy response. *Proc. Natl. Acad. Sci. U. S. A.* **118**, e2103240118
28. Platanitis, E., and Decker, T. (2018) Regulatory networks involving STATs, IRFs, and NFκB in inflammation. *Front. Immunol.* **9**, 2542
29. Hu, J., Schokrpur, S., Archang, M., Hermann, K., Sharrow, A. C., Khanna, P., *et al.* (2018) A non-integrating lentiviral approach overcomes cas9-induced immune rejection to establish an immunocompetent metastatic renal cancer model. *Mol. Ther. Methods Clin. Dev.* **9**, 203–210
30. Schokrpur, S., Hu, J., Moughon, D. L., Liu, P., Lin, L. C., Hermann, K., *et al.* (2016) CRISPR-mediated VHL knockout generates an improved model for metastatic renal cell carcinoma. *Sci. Rep.* **6**, 29032
31. Yasuda, S., Morokawa, N., Wong, G. W., Rossi, A., Madhusudhan, M. S., Sali, A., *et al.* (2005) Urokinase-type plasminogen activator is a preferred substrate of the human epithelium serine protease tryptase epsilon/PRSS22. *Blood* **105**, 3893–3901
32. Santibanez, J. F., Obradović, H., Kukolj, T., and Krstić, J. (2018) Transforming growth factor-β, matrix metalloproteinases, and urokinase-type plasminogen activator interaction in the cancer epithelial to mesenchymal transition. *Dev. Dyn.* **247**, 382–395
33. Li, S., Wei, X., He, J., Tian, X., Yuan, S., and Sun, L. (2018) Plasminogen activator inhibitor-1 in cancer research. *Biomed. Pharmacother.* **105**, 83–94
34. Dellas, C., and Loskutoff, D. J. (2005) Historical analysis of PAI-1 from its discovery to its potential role in cell motility and disease. *Thromb. Haemost.* **93**, 631–640
35. Teng, F., Zhang, J. X., Chen, Y., Shen, X. D., Su, C., Guo, Y. J., *et al.* (2021) LncRNA NKX2-1-AS1 promotes tumor progression and angiogenesis via upregulation of SERPINE1 expression and activation of the VEGFR-2 signaling pathway in gastric cancer. *Mol. Oncol.* **15**, 1234–1255
36. Jouan, V., Canron, X., Alemany, M., Caen, J. P., Quentin, G., Plouet, J., *et al.* (1999) Inhibition of *in vitro* angiogenesis by platelet factor-4-derived peptides and mechanism of action. *Blood* **94**, 984–993
37. O'Reilly, M. S., Boehm, T., Shing, Y., Fukai, N., Vasios, G., Lane, W. S., *et al.* (1997) Endostatin: an endogenous inhibitor of angiogenesis and tumor growth. *Cell* **88**, 277–285
38. Lord, M. S., Cheng, B., Farrugia, B. L., McCarthy, S., and Whitelock, J. M. (2017) Platelet factor 4 binds to vascular proteoglycans and controls both growth factor activities and platelet activation. *J. Biol. Chem.* **292**, 4054–4063
39. Huang, L., Fang, X., Shi, D., Yao, S., Wu, W., Fang, Q., *et al.* (2020) MSP-RON pathway: potential regulator of inflammation and innate immunity. *Front. Immunol.* **11**, 569082
40. Millar, R., Kilbey, A., Remak, S. J., Severson, T. M., Dhayade, S., Sandilands, E., *et al.* (2020) The MSP-RON axis stimulates cancer cell growth in models of triple negative breast cancer. *Mol. Oncol.* **14**, 1868–1880
41. Huang, Z., Liu, X., Wu, C., Lu, S., Antony, S., Zhou, W., *et al.* (2021) A new strategy to identify ceRNA-based CCDC144NL-AS1/SERPINE1 regulatory axis as a novel prognostic biomarker for stomach adenocarcinoma via high throughput transcriptome data mining and computational verification. *Front. Oncol.* **11**, 802727
42. Schoppmeyer, R., Zhao, R., Cheng, H., Hamed, M., Liu, C., Zhou, X., *et al.* (2017) Human profilin 1 is a negative regulator of CTL mediated cell-killing and migration. *Eur. J. Immunol.* **47**, 1562–1572
43. Yetkin-Arik, B., Vogels, I. M. C., Nowak-Sliwinska, P., Weiss, A., Houtkooper, R. H., Van Noorden, C. J. F., *et al.* (2019) The role of glycolysis and mitochondrial respiration in the formation and functioning of endothelial tip cells during angiogenesis. *Sci. Rep.* **9**, 12608
44. Goldman, M. J., Craft, B., Hastie, M., Repečka, K., McDade, F., Kamath, A., *et al.* (2020) Visualizing and interpreting cancer genomics data via the Xena platform. *Nat. Biotechnol.* **38**, 675–678
45. Hao, Y., Hao, S., Andersen-Nissen, E., Mauck, W. M., 3rd, Zheng, S., Butler, A., *et al.* (2021) Integrated analysis of multimodal single-cell data. *Cell* **184**, 3573–3587.e3529
46. Korsunsky, I., Millard, N., Fan, J., Slowikowski, K., Zhang, F., Wei, K., *et al.* (2019) Fast, sensitive and accurate integration of single-cell data with Harmony. *Nat. Methods* **16**, 1289–1296
47. Newman, A. M., Steen, C. B., Liu, C. L., Gentles, A. J., Chaudhuri, A. A., Scherer, F., *et al.* (2019) Determining cell type abundance and expression from bulk tissues with digital cytometry. *Nat. Biotechnol.* **37**, 773–782
48. Schürch, C. M., Bhate, S. S., Barlow, G. L., Phillips, D. J., Noti, L., Zlobec, I., *et al.* (2020) Coordinated cellular neighborhoods orchestrate antitumoral immunity at the colorectal cancer invasive front. *Cell* **182**, 1341–1359.e1319